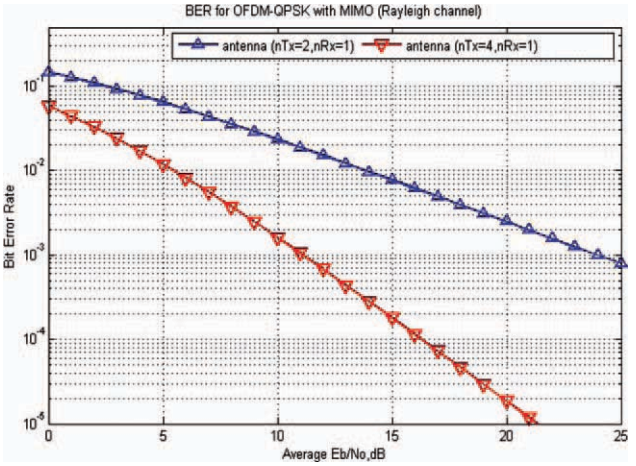

Figure 3 BER v/s SNR plot for Rayleigh channel with MIMO OFDM-QPSK system. [Color figure can be viewed in the online issue, which is available at wileyonlinelibrary.com]

spectra diagrams of RZ-DPSK signal before transmission are shown in Figures 2(a) and 2(b), respectively. In our scheme, a RZ-DPSK with 50% duty cycle is generated via a MZM cascaded by a PM [11], as shown in Figure 2(a). The received eye diagram of RZ-DPSK signal after 106 km transmission over 90 km SSMF and 16 km DCF is shown in Figure 2(c), and the eye is clear open. Q factor v/s bit period for RZ-DPSK signal is shown in Figure 2(d), Q factor value is perfect while 3R signal process is performed and the decision point of the demodulated signal is 0.5 bit time. Hence, the received signal can be efficiently converted into a binary form and then modulated again so that it can be used as an input to the transmitters of the MIMO-OFDM system. The BER v/s SNR curves for the systems with two transmit antennas and four transmit tested with the Rayleigh channels are shown in Figure 3. It can be seen that BER performance of almost 10^{-3} is achieved at SNR of 11 dB with four transmit antennas and one receive antenna which is better as compared to two transmit antennas and one receive antenna. Hence, the system with two transmit antennas is better than four transmit antennas for one receive antenna MIMO-OFDM system and both of them is found to be within acceptable BER limits.

4. CONCLUSIONS

In this article, seamless integration of RZ-DPSK-DWDM optical links with MIMO-OFDM system for fourth generation wide-area coverage mobile communication is proposed and demonstrated. The long distance transmission for RZ-DPSK WDM is done, and the demodulated RZ-DPSK signal is transformed to the binary data, which is given to MIMO-OFDM-QPSK wireless communication system. Two MIMO-OFDM-QPSK wireless system is designed with two transmit antennas and one receive antenna and four transmit antennas and one receive antenna. Results prove the BER performance of almost 10^{-3} is achieved at SNR of 11 dB with four transmit antennas and one receive antenna which is better as compared to two transmit antennas and one receive antenna. The proposed system with two transmit antennas is better than four transmit antennas for one receive antenna MIMO-OFDM system and both of them is found to be within acceptable BER limits. Because this scheme is not complex and the cost budget is cheap, it is a competitive scheme in the future fourth generation wide-area coverage mobile communication.

ACKNOWLEDGMENTS

This work was partially supported by the National High Technology Research and Development Program (973) of China (Grant No. 2010CB328300), National Natural Science Foundation of China (Grant Nos. 61107064, 61177071, 600837004, 60777010), Doctoral Fund of Ministry of Education, Open Fund of State Key Lab of ASIC & System (Grant No. 11MS009), Pujiang Fund, and Shuguang fund.

REFERENCES

1. Special issue on IMT-2000, Standards efforts of the ITU, IEEE Pers Commun 4 (1997), 8–40.
2. http://www.itu.int/home/imt.html
3. A. Goel and R.S. Mishra, Remote data acquisition using wireless SCADA system, Int J Eng 3 (2009), 58–65.
4. Y. Shao, N. Chi, J. Zhang, W. Fang, B. Huang, and L. Tao, A novel scheme for seamless integration of ROF system with OFDM-CPM WDM passive optical network, Presented at the IEEE Optical Fiber Communication Conference and Exposition (OFC), OWT4, 2011.
5. Y. Shao, B. Huang, N. Chi, J. Zhang, W. Fang, B. Liu, and X. Xin, A novel subcarrier OFDM-MSK WDM passive optical network, Presented at the IEEE Optical Fiber Communication Conference and Exposition (OFC), OTuO4, 2010.
6. Y. Shao and N. Chi, Generation of OFDM-MSK signal and its application for radio over fiber system in future access network, Presented at the IEEE CMC, 2011, pp. 206–209.
7. Y. Shao, J. Zhang, B. Huang, J. Zhu, W. Fang, and X. Li, A novel OFDM-CPM modulation scheme and its application in WDM-PON, Chin Opt Lett 8 (2010), 894–898.
8. J. Zhu, S. Wen, Y. Shao, H. Wen, and Z. Wang, Full diversity concatenation space-time coding over time-selective block Rayleigh fading channels via duality, Presented at the IEEE WiCOM, 2006, pp. 1–5.
9. A.J. Paulraj, R.U. Nabar, and D.A. Gore, Introduction to space-time wireless communications, Cambridge, UK, Cambridge University Press, 2003.
10. S. Almouti, A simple transmit diversity technique for wireless communication, IEEE J Select Areas Commun 16 (1998), 1451–1458.
11. Y. Shao, N. Chi, C. Hou, et al., A novel return-to-zero FSK format for 40-Gb/s transmission system applications, IEEE J Lightwave Technol 28 (2010), 1770–1782.

SENSING OF HYDROSTATIC PRESSURE USING FBG SENSOR FOR LIQUID LEVEL MEASUREMENT

D. Sengupta, M. Sai Shankar, P. Saidi Reddy, R. L. N. Sai Prasad, and K. Srimannarayana
Department of Physics, National Institute of Technology, Waranagal 506 004, Andra Pradesh, India; Corresponding author: mb2shankar@yahoo.co.in

Received 12 September 2011

ABSTRACT: *Pressure and temperature are two important parameters in hydrostatic pressure based liquid level sensing. In this study, we propose a liquid level sensor based on hydrostatic pressure variation sensed by fiber Bragg grating (FBG1) attached to a bourdon tube. The water column pressure sensitivity coefficient of FBG1 is 0.072 nm/m. One more FBG2 is incorporated to avoid cross sensitivity of temperature. The temperature sensitivity coefficient of the FBG1 and FBG2 are 10.5 pm/°C and 10.2 pm/°C. The packaged sensor head can*

be placed inside a chamber and also easily mountable external to the tank for the measurement of liquid level. © 2012 Wiley Periodicals, Inc. Microwave Opt Technol Lett 54:1679–1683, 2012; View this article online at wileyonlinelibrary.com. DOI 10.1002/mop.26890

Key words: *FBG sensor; liquid level; hydrostatic pressure; temperature; Bourdon tube*

1. INTRODUCTION

Pressure and temperature are two important parameters for liquid level measurement through hydrostatic pressure sensing. Electronic sensors such as quartz pressure gauges allow only single point measurements and are limited in temperature range of operation and these are commercial available. Furthermore their long-term reliability in harsh environment is relatively poor. Fiber-optic sensors can be used in the harsh environments for permanent monitoring of temperature and pressure [1]. Extrinsic Fabry–Perot interferometer-based optical fiber sensors have been successfully applied to the hydrostatic pressure and temperature measurements in recent years [2, 3]. Fiber Bragg grating (FBG) based sensors offer a number of inherent advantages such as the possibility of quasi distributed measurements along a single fiber, long distance passive signal recovery, and a wavelength encoded output, which requires no referencing. Bare FBG based pressure sensor is capable of sensing pressure directly with low-pressure sensitivity and is easy to be multiplexed in series [4]. To enhance the pressure sensitivity several techniques were proposed [5–10]. FBG sensors can be used for hydrostatic pressure sensing in industrial application. But FBG has higher temperature–pressure cross sensitivity. Several models were demonstrated to compensate the temperature effect during strain or pressure measurement [11]. A bourdon tube based water level sensor using two inline FBGs were demonstrated by Fukuchi et al. The sensor head consists of a bourdon tube with diaphragm and two inline FBGs. The full water level range of this arrangement is 10 m only [12].

In this study, a simple sensor head consist of a bourdon tube and two inline FBGs is proposed for liquid level measurement.

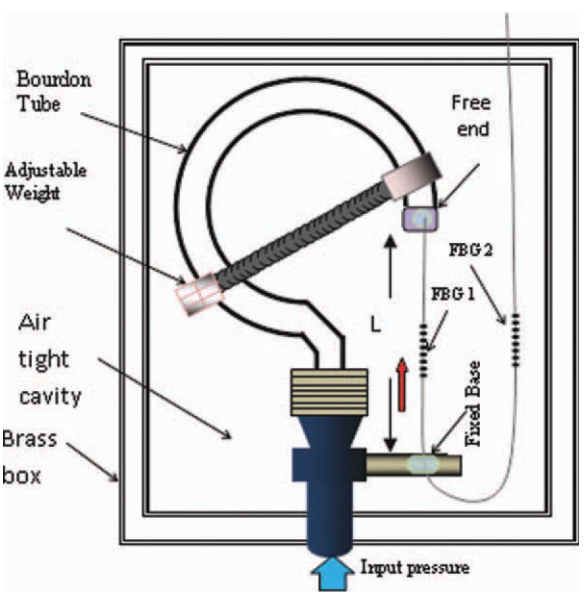

Figure 1 Schematic structure of hydrostatic pressure sensor head. [Color figure can be viewed in the online issue, which is available at wileyonlinelibrary.com]

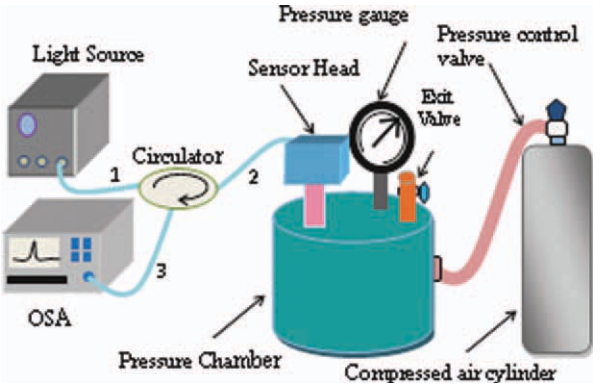

Figure 2 Schematic experimental setup for pressure sensing. [Color figure can be viewed in the online issue, which is available at wileyonlinelibrary.com]

The water column pressure sensitivity coefficient of the sensor is 0.072 nm/m with 99% linearity. Portable and simple design of the sensor head can be used to monitor hydrostatic pressure and liquid level present in a tank.

2. SENSOR HEAD DESIGN AND PRINCIPLE

The sensor head consists of a ''C'' shape bourdon tube of a pressure gauge and an optical fiber with two FBGs written inline are used.

This bourdon tube has an elliptical cross section and its free end is sealed. The tube tends to straighten out on the application of pressure and the angular deflection of the free end is taken as a measure of the pressure. The deflection of a bourdon tube varies with the ratio of its major to minor cross sectional axis, there is also a tube length difference between the internal and external pressures, and radius of curvature. It also varies inversely with the tube-wall thickness and the modulus of elasticity of the material used. Bourdon tubes are fabricated with the material which has stable elastic properties to suit the fluid for which the pressure is to be measured. Phosphor bronze, beryllium copper, and stainless steel are used most widely, but for applications involving particularly corrosive fluid, alloys such K-Monel is used.

The empirical formula for the free end tip displacement Δl of bourdon tube with applied pressure P is [13].

$$\Delta l = 0.05\frac{SP}{E}\left(\frac{D}{t}\right)^{0.2}\left(\frac{w_1}{w_2}\right)^{0.33}\left(\frac{w_1}{t}\right)^{3} \quad (1)$$

where w_1, w_2, t, D, S, and E are the major and minor axis of elliptical cross section of the bourdon tube, thickness of the of the bourdon tube, diameter of the C shape bourdon tube, circumferential length, and Young modulus of the bourdon tube, respectively, and P is the applied pressure.

The region of the fiber where one FBG (FBG1) is written is glued in between the tip of the free end and the fixed base of the bourdon tube Figure 1.

The displacement of the free end due to change in pressure induces strain in the FBG1. The strain response of FBG1 arises due to both the physical elongation of the grating (fractional change in grating pitch), and the change in fiber index due to photo elastic effects, whereas the thermal response arises due to the inherent thermal expansion of the fiber material and the temperature dependence of the refractive index. The relative change in Bragg wavelength with strain and temperature can be expressed as

$$\frac{\Delta\lambda_{B1}}{\lambda_{B1}} = (1 - P_e)\varepsilon_{ax} + (\alpha_s + \zeta_s)\Delta T \quad (2)$$

where ε_{ax} is the axially applied strain, P_e is the effective photo elastic constant (0.22) of the fiber material, ΔT is the change in temperature, α_s and ζ_s are the thermal expansion and thermal optic coefficients of the fiber material. The subscript "s" represents silica fiber. λ_{B1} is the Bragg wavelength of FBG1.

For an FBG under axial strain, the shift in the Bragg wavelength at constant temperature is

$$\frac{\Delta\lambda_{B1}}{\lambda_{B1}} = (1 - P_e)\varepsilon_{ax} \quad (3)$$

The axial strain experienced by the FBG1 is expressed as

$$\varepsilon_{ax} = \frac{\Delta L}{L} \quad (4)$$

where "L" is the length of the fiber between free end and fixed end of the bourdon tube. ΔL is the change in length of the length of the fiber.

With the deflection of the bourdon tube due to applied pressure, the strain experienced by the FBG1 is

$$\varepsilon_{ax} = \eta\frac{\Delta l}{L} \quad (5)$$

where "η" is a rational factor that correlates the ΔL and Δl.

Combining Eqs. (1), (3), and (5) the Bragg wavelength shift of FBG1 with applied pressure is

$$\frac{\Delta\lambda_{B1}}{\lambda_{B1}} = (1 - P_e)\frac{\eta}{L}0.05\frac{SP}{E}\left(\frac{D}{t}\right)^{0.2}\left(\frac{w_1}{w_2}\right)^{0.33}\left(\frac{w_1}{t}\right)^{3} \quad (6)$$

The pressure sensitivity of the FBG1 is 50 pm/psi measured theoretically. For pure strain measurements using FBG1, effects of temperature change on the Bragg wavelength has to be suitably compensated since it is sensitive to temperature also. A second FBG (FBG2) is incorporated to compensate the temperature effect experienced by the FBG1. Unlike the FBG1 the FBG2 is free from strain. As a result no Bragg wavelength shift from FBG2 occurs when there is a change in pressure. The change in temperature effects the shift in Bragg wavelength of FBG1 and FBG2 and is given by

$$\frac{\Delta\lambda_{B(i)}}{\lambda_{B(i)}} = (\alpha + \zeta)\Delta T \quad (7)$$

where $i = 1,2$. Furthermore by measuring $\Delta\lambda_{B1}$ and $\Delta\lambda_{B2}$ from FBG1 and FBG2 due to change in pressure and temperature, simultaneous measurement of pressure and temperature can be determined using Eqs. (2) and (7). Since the FBG1 and FBG2 have very different responses to pressure and temperature, a matrix equation can be written and inverted to yield pressure and temperature from measurements of the $\Delta\lambda_{B1}$ and $\Delta\lambda_{B2}$.

$$\begin{pmatrix}\Delta P\\ \Delta T\end{pmatrix} = \frac{1}{Z}\begin{pmatrix}K_{T_2} & -K_{T_1}\\ -K_{P_2} & K_{P_1}\end{pmatrix}\begin{pmatrix}\Delta\lambda_{B1}\\ \Delta\lambda_{B2}\end{pmatrix} \quad (8)$$

where $Z = K_{P1}K_{T2} - K_{T1}K_{P2}$, K_{P1}, K_{T1} and K_{P2}, K_{T2} are the pressure and temperature sensitivity coefficients of FBG_1 and FBG_2, respectively. In practice the elements of the matrix K_{pi} and K_{Ti} $(i = 1,2)$ can be determined experimentally by measuring separately the Bragg wavelength shifts with pressure and temperature.

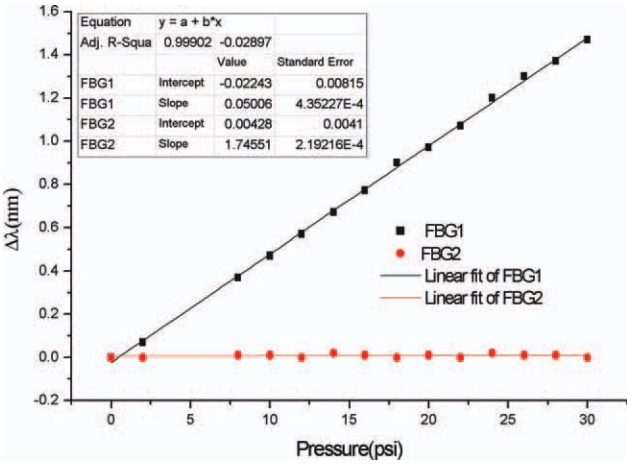

Figure 3 Response of FBG1 and FBG2 with the applied pressure. [Color figure can be viewed in the online issue, which is available at wileyonlinelibrary.com]

Substituting 1 MPa = 102 m water column pressure, the shift in Bragg wavelength with the water column pressure is

$$\frac{\Delta\lambda_{B1}}{\lambda_{B1}} = 102H(1 - P_e)\frac{\eta}{L}0.05\frac{S}{E}\left(\frac{D}{t}\right)^{0.2}\left(\frac{w_1}{w_2}\right)^{0.33}\left(\frac{w_1}{t}\right)^{3} \quad (9)$$

where "H" represents the water level present above the sensor head in meters.

3. EXPERIMENTAL SETUP AND RESULTS

Figure 2 shows schematic experimental setup for pressure sensing. It consists of a sensor head, light source, circulator, optical spectrum analyzer (OSA), pressure gauge, pressure chamber, pressure controlling valve, and compressed air cylinder.

The sensor head consist of a C shape bourdon tube made up of brass ($t = 0.5$ mm, $D = 38$ mm, $S = 74$ mm, $w_1 = 12$ mm, and $w_2 = 2.4$ mm). The maximum pressure applied to the bourdon tube is limited to elastic range of the transducer material and fiber sensor. The elastic limit of the bourdon tube material corresponds to about 40% of the yield strength. An adjustable weight is used because the bourdon tube has a relatively low restoring force. It also protects in a limited way against overloading by supporting the elastic element at a specific pressure limit.

FBG1 and FBG2 in the sensor head are of 3 mm length written on the same fiber. The resonant peaks λ_{B1} and λ_{B2} of FBG1 and FBG2 are 1545.83 nm and 1543.01 nm, respectively. The length between the free end and a fixed support of the bourdon tube is $L = 4$ cm. The inline FBG2 is free from strain and kept inside the sensor head. The bourdon tube arrangement is enclosed in a sealed box made of brass to isolate it from surrounding atmosphere.

Light from a broad band source (50 nm bandwidth and 6 mW of power) illuminates the FBGs via circulator, and an OSA (Agilent 86142B) was used to measure the Bragg wavelength shift by monitoring the reflection spectrum of the gratings.

Pressure chamber is made up of stainless steel (diameter 15 cm and height 10 cm) which can hold pressure upto 100 psi. A pressure control valve is arranged to control the pressure. A

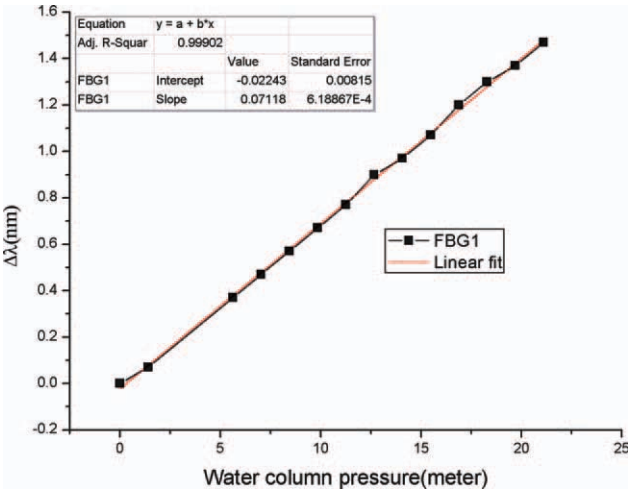

Figure 4 Response of FBG1 with water column pressure. [Color figure can be viewed in the online issue, which is available at wileyonlinelibrary.com]

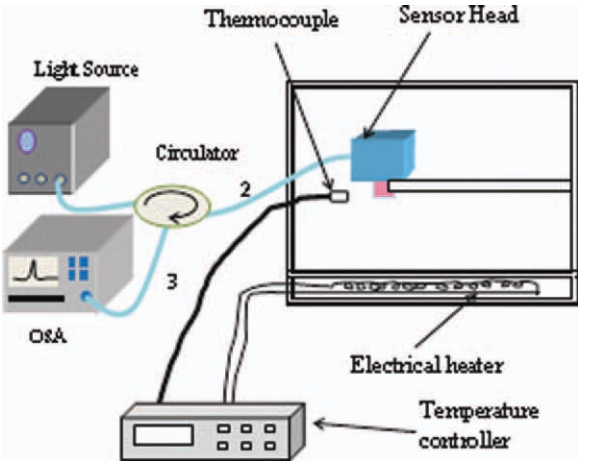

Figure 6 Schematic experimental setup for temperature sensing. [Color figure can be viewed in the online issue, which is available at wileyonlinelibrary.com]

pressure gauge is attached to the chamber to measure the pressure. A compressed air cylinder is attached to the pressure chamber and with help of a control valve pressure in the pressure chamber is adjusted.

With the release of air from the compressed gas cylinder the pressure in chamber increases. Because of this the displacements of free end of the bourdon tube takes place and FBG1 experiences strain. The change in strain shift the λ_{B1} and is measured using OSA.

The experimental results of λ_{B1} and λ_{B2} to applied pressure ($P = 0$ to 30 psi) at constant room temperature is plotted Figure 3. The shift in Bragg wavelength per unit applied pressure of FBG1 is found to be 50.05×10^{-3} nm/psi. It is around 2388 times higher than bare FBG [4]. This corresponds to a pressure sensitivity of 0.0032×10^{-2}/psi and there is no shift in λ_{B2} and it is as expected. The corresponding "η" in Eq. (5) is 0.04 and is calculated from experimental result.

The results obtained from the above experiment are utilised and converted to its equivalent water column pressure. The corresponding wavelength shift is plotted with water column pressure Figure 4.

The experiment was conducted for many times within the pressure range 0 to 30 psi which is equal to 21.092 m of water column pressure. Considering two trials (Trial1 and Trial2) for this sensing range, the response of the λ_{B1} shows a significantly narrow difference between this two trials Figure 5. Trial1 and Trail2 represent the response of the λ_{B1} with increasing and decreasing of the applied pressure. During the experiment a non linear shift is observed in between 20 and 25 psi due to external vibration and this can be reduced by filling air tight with silicone oil Figure 5.

To measure the temperature response of λ_{B1} and λ_{B2}, the sensor head is kept in a temperature controlled chamber (oven) at normal atmospheric pressure Figure 6. A "K" type thermo couple is used to measure temperature.

The temperature response of λ_{B1} and λ_{B2} within the temperature range $T = 30°C$ to 100°C is shown in Figure 7. The λ_{B1} and λ_{B2} are shifted to longer wavelength linearly with increasing temperature.

The measured temperature sensitivity coefficients of λ_{B1} and λ_{B2} are 10.5 pm/°C and 10.2 pm/°C, respectively, Figure 7.

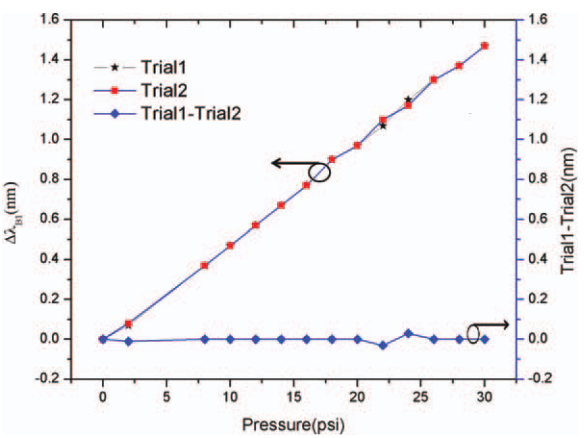

Figure 5 Response of FBG1 with increase and decrease in pressure. [Color figure can be viewed in the online issue, which is available at wileyonlinelibrary.com]

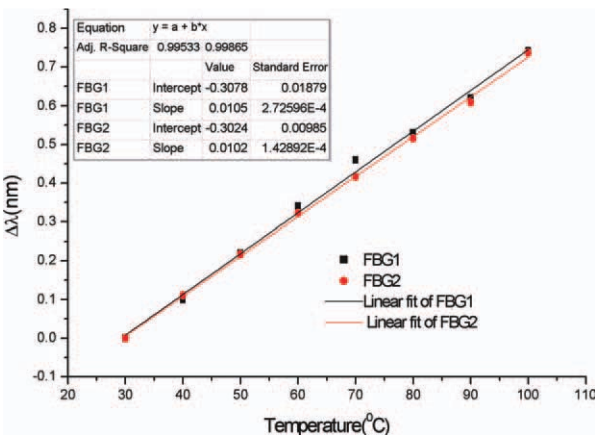

Figure 7 Response of λB1 and λB2 with temperature. [Color figure can be viewed in the online issue, which is available at wileyonlinelibrary.com]

Pressure and temperature responses of λ_{B1} and λ_{B2} are measured by independently applying strain and temperature to the sensor head. The pressure and temperature sensitivity coefficients of λ_{B1} and λ_{B2} obtained from the experimental results are $K_{p1} = 50.05 \times 10^{-3}$ nm/psi, $K_{T1} = 10.5$ pm/°C, $K_{p2} = 0$ nm/psi, and $K_{T2} = 10.2$ pm/°C, respectively.

Using the pressure and temperature sensitivity coefficients of λ_{B1} and λ_{B2} from Figures 3 and 7. Results can be written in vector form and by inverting the sensitivity matrix, simultaneous measurement of pressure and temperature can be measured.

$$\begin{pmatrix} \Delta P \\ \Delta T \end{pmatrix} = \frac{1}{501.601} \begin{pmatrix} 10.2 & 10.5 \\ 0 & 50.06 \end{pmatrix} \begin{pmatrix} \Delta\lambda_{B1} \\ \Delta\lambda_{B2} \end{pmatrix} \quad (10)$$

where ΔP and ΔT are change in pressure and temperature, respectively. The preliminary results have demonstrated that the sensing head can perform simultaneous measurement of pressure and temperature. The maximum experimental errors obtained are ±0.5 psi and ±3°C, within the pressure (0–30 psi) and temperature (0–100°C) range essentially determined by the resolution of the OSA. In principle, better resolution can be achieved if more sensitive FBG interrogation schemes are utilized.

4. CONCLUSION

In this experiment there are two FBG sensors, FBG1 bonded between free end and the fixed base of the bourdon tube and the FBG2 is free from strain. The bourdon tube converts the applied pressure into axial strain in the FBG1. The pressure sensitivity coefficient of FBG1 and FBG2 are 50.06 pm/psi and 0 pm/psi experimentally measured. The FBG2 is included for temperature compensation because FBG sensor has temperature cross sensitivity.

Though the response of FBG1 to the applied pressure is low i.e. 0.072 nm/m in this sensor head arrangement, it can be used to measure water level present in bore well and liquid level in pressurized vessel in industries.

ACKNOWLEDGMENTS

The authors thank Prof. S. Asokan, Indian Institute of Science, Bangalore, India for permitting to use the FBG facility.

REFERENCES

1. A. Wang et al., Self-calibrated interferometric-intensity-based optical fiber sensors, J Lightwave Technol 19 (2001), 529–551.
2. Q. Wang, L. Zhang, C. Sun, and Q. Yu, Multiplexed fiber optic pressure and temperature sensor system for down hole measurement IEEE Sens J 8 (2008), 1879–1883.
3. S. H. Aref, H. Latifi, M. I. Zibaii, and M. Afshari, Fiber optic Fabry-Perot pressure sensor with low sensitivity to temperature changes for downhole application, Opt Commun 269 (2007), 322–330.
4. M. G. Xu, L. Reekie, Y. T. Chow, and J. P. Dakin, Optical in fibre grating high pressure sensor, Electron Lett 29 (1993), 398–399.
5. M. G. Xu, H. Geiger, and J. P. Dakin, Fibre grating pressure sensor with enhanced sensitivity using a glass bubble housing, Electron Lett 32 (1996), 128–129.
6. Y. Liu, Z. Guo, Y. Zhang, K. S. Chiang, and X, dong, Simultaneous pressure and temperature measurement with polymer coated fibre Bragg grating, Electron Lett 36 (2000), 564–566.
7. H.-J. Sheng, M.-Y. Fu, T.-C. Chen, W.-F. Liu, and S.-S. Bor, A lateral pressure sensor using a fiber bragg grating, IEEE Photonics Technol Lett 16 (2004), 1146–1148.
8. L. H. Liu, H. Zhang, Q. Zhao, Y. Liu, and F. Li, Temperature independent FBG pressure sensor with high sensitivity, Opt Fiber Technol 13 (2007), 78–80.
9. W. T. Zhang, F. Li, Y. L. Liu, and L. H. LIu, Ultrathin FBG pressure sensor with enhanced responsitivity, IEEE Photonics Technol Lett 19 (2007).
10. L. Liu, Y. Li, Y. He, F. Li, and Y. Liu, Membrane based fiber bragg grating pressure sensor with high sensitivity, Microwave Opt Technol Lett 51 (2009).
11. M. Majumder, T. K. Gangopadhay, A. K. Chakraborty, K. Dasgupta, and D. K. Bhatacharya, Fibre Bragg gratings in structural health monitoring—Present status and applications, Sens Actuators A: Phys 147 (2008), 150–164.
12. K. Fukuchi, S. Kojima, Y. Hishida, and S. Lshi, Optical water level sensors using fiber Bragg grating technology, Hitachi Cable Rev (2002), Japan, 23–28.
13. J. Prasad, M. N. Jayaswal, and V. Priye, Instrumentation and process control, 17.

TWO-POLES COMPACT MICROSTRIP BANDPASS FILTER WITH SHARP TRANSITION BANDS USING HIGH PERMITTIVITY SUBSTRATE

Wen-Ruei Yang and Cheng-Liang Huang
Department of Electrical Engineering, National Cheng Kung University, 1 University Rd., Tainan 70101, Taiwan, Republic of China; Corresponding author: u8923034@hotmail.com

Received 15 September 2011

ABSTRACT: *This article describes the two-pole microstrip band-pass filters using miniaturized center-stubbed open stubs and tapped-line input/output ports. The two-poles bandpass filters by using FR4 and high-permittivity ceramic substrates (with respective dielectric constants of 4.5 and 31.55) are investigated. Microwave dielectric ceramics with high permittivity are commonly applied in several microwave communication components. The advantage of using high permittivity ceramic substrates is to reduce the sizes and increase the performance of microstrip bandpass filters. The responses of the filters using FR4 ($\varepsilon_r = 4.5$, tan $\delta = 0.015$) and $Nd(Zn_{1/2}Ti_{1/2})O_3$ ($\varepsilon_r = 31.55$, tan $\delta = 0.00005$) ceramic substrates are designed at a center frequency of 2 GHz. The compact size, low-loss, sharp response, and performance of the filter are presented in this article.* © 2012 Wiley Periodicals, Inc.

Microwave Opt Technol Lett 54:1683–1686, 2012; View this article online at wileyonlinelibrary.com. DOI 10.1002/mop.26889

Key words: *high permittivity; band-pass filter*

1. INTRODUCTION

In the next generation of mobile and satellite communication systems, the characteristics of compact size and high-performance for modern microwave filters are highly needed to reduce cost and improve system performance. To achieve the compact size and sharp transition bands, the compact bandpass filter using a miniaturized center-stubbed half-wavelength resonator is a good choice [1].

They can be designed in many different ways and by using different materials. Ceramic material with a high quality factor ($Q \times f$) value (>100,000) and a high permittivity provides a means to create small resonator structures, such as coaxial structures, that can be coupled to form combline bandpass filters [2]. However, further miniaturization becomes more difficult for this filter. Planar filters using high-permittivity ceramic substrate provide good miniaturization ability [3–6]. Therefore, much research has been conducted on planar filters and their components.